Available online at www.sciencedirect.com
SCIENCE DIRECT®
Precambrian Research 132 (2004) 327–348
Precambrian Research
www.elsevier.com/locate/precamres

P–T history of garnet-websterites in the Sharyzhalgai complex, southwestern margin of Siberian craton: evidence for Paleoproterozoic high-pressure metamorphism

Tsutomu Ota [a,*], Dmitry P. Gladkochub [b], Eugene V. Sklyarov [b], Anatoly M. Mazukabzov [b], Teruo Watanabe [c,1]

[a] *Department of Earth and Planetary Sciences, Tokyo Institute of Technology, Tokyo 152-8551, Japan*
[b] *Institute of the Earth's crust, Russian Academy of Sciences, Irkutsk 664033, Russia*
[c] *Division of Earth and Planetary Sciences, Graduate School of Science, Hokkaido University, Sapporo 060-0810, Japan*

Received 11 December 2002; accepted 4 March 2004

Abstract

The Saramta massif in the Paleoproterozoic Sharyzhalgai complex, the southwestern margin of the Siberian craton, is mainly composed of spinel-peridotites with garnet-websterites; it is enclosed within granitic gneisses and migmatites with mafic intercalations of granulite-facies grade. The garnet-websterites occur as lenses or layers intercalated within spinel-harzburgite and spinel-lherzolite. They consist mainly of clinopyroxene (Cpx), garnet (Grt), and orthopyroxene (Opx): Grt often includes Cpx, Opx, and pargasite (Prg). Opx also occurs as kelyphite with plagioclase (Pl), spinel, olivine, Prg, and biotite. Relationships between textures and chemical compositions of these minerals suggest the following *P–T* stages: stage 1 (pre-peak), 0.9–1.5 GPa at 640–780 °C; stage 2 (peak), 2.3–3.0 GPa at 920–1030 °C as the minimum estimate; and stage 3 (post-peak), 750–830 °C at 0.5–0.9 GPa. Finally, the garnet-websterites are veined with lower amphibolite- to greenschist-facies minerals (stage 4).

These results suggests that the Saramta massif was carried to depths of c. 100 km by subduction, and metamorphosed under eclogite-facies conditions in the Paleoproterozoic, despite the commonly held view that high geothermal gradients in those times would have prevented such deep subduction. Paleoproterozoic plate subduction at the southwestern margin of the Siberian craton might have caused subduction-zone magmatism and mantle metasomatism similar to those in the Phanerozoic.

Keywords: Paleoproterozoic; High-pressure metamorphism; Garnet-websterites; Siberia; Tectonics

1. Introduction

High-pressure (HP) metamorphic rocks provide valuable information on deep tectonic processes within orogenic belts. The evolution of garnet-bearing ultramafic HP rocks including orogenic peridotites and pyroxenites, have been used to monitor subduction and various aspects of orogenic and collision processes within various orogens (e.g., Liou et al., 1994; Brueckner, 1998; Zhang and Liou, 1998; Brueckner and Medaris, 2000). These rocks can be formed by various processes. In an active convergent margin, high-temperature spinel-bearing ultramafic rocks can crystallize at near-solidus temperatures and subse-

* Corresponding author. Present address: Institute for Study of the Earth's Interior, Okayama University, Misasa, Tottori 682-0193, Japan. Fax: +81-858-43-3795.
E-mail address: tsutom@pheasant.misasa.okayama-u.ac.jp (T. Ota).
[1] Deceased, May 9, 2002.

0301-9268/$ – see front matter © 2004 Elsevier B.V. All rights reserved.
doi:10.1016/j.precamres.2004.03.009

quently become refrigerated into the garnet stability field; this cooling process may be accompanied with further burial by plate subduction or counter-flow in the mantle wedge. In other cases, these lithologies may be generated by prograde HP metamorphism of either spinel-peridotites or serpentinites that had previously been incorporated into the crust as parts of ophiolite complexes. Distinction between these different origins is essential for unraveling the complex tectonothermal histories of orogenic belts. One promising approach is the establishment of *P–T*-time paths based on mineralogical data, geothermobarometric calculations, and isotope dating.

In addition, plate subduction into the deep mantle plays an important role for crustal and mantle evolution of the Earth, because oceanic crustal materials, hydrothermally altered at the mid-ocean ridge, brought into mantle depths by the plate subduction greatly influence subduction-zone magmatism and mantle metasomatism. In general, high geothermal gradients in the Precambrian are thought to have hampered plate subduction to depths appropriate to blueschist- and eclogite-facies HP metamorphism, which is a feature of the Phanerozoic plate tectonics. When the Phanerozoic-type plate tectonics initiated is one of the most important clues in order to understand the whole mantle dynamics and its history.

The Sharyzhalgai complex is situated on the southwestern margin of the Siberian craton, and is comprised of granulite-facies grade mafic and ultramafic rocks (the Saramta massif) enclosed within migmatitic gneisses. The ultramafic rocks contain lenses of garnet-websterite. The high-grade metamorphic rocks have previously been investigated in terms of igneous and metamorphic petrology, structural geology, and geochronology (e.g., Aftalion et al., 1991; Khiltova, 1993; Gornova and Petrova, 1999; Sklyarov et al., 1998, 2001). These studies have revealed that Archean protoliths were subjected to two periods of granulite-facies metamorphism; the first one with formation of enderbite, charnokite, and kinzigite during late Archean to early Paleoproterozoic, and the second accompanied by extensive migmatization during late Paleoproterozoic. Igneous petrology and geochemical studies of the mafic granulites and ultramafic rocks (Gornova and Petrova, 1999) indicate that their protoliths were basaltic rocks with mid-ocean ridge basalt (MORB) compositions, and partially-molten sub-oceanic mantle, respectively, and together could represent a fragment of Archean oceanic crust and underlying mantle. However, previous petrochemical studies indicate that the ultramafic rocks (pyroxenites) crystallized at pressure conditions over 2 GPa (Gornova and Petrova, 1999). Such conditions are unusually high for those of mid-ocean ridge magmatism, even allowing for the fact that the pre-Mesoproterozoic oceanic crust may have been two or three times as thick as at present (e.g., Moores, 1986, 1993, 2002). Another unresolved issue concerns the nature and timing of the juxtaposition between the mafic/ultramafic lithologies and the gneiss complex.

The aim of this paper is to describe the petrographic and metamorphic mineralogical characteristics of the garnet-websterites in order to investigate the tectonothermal history of the Saramta massif and its relationship with the adjacent granulite-gneiss complex, and to discuss their implications to Paleoproterozoic plate tectonics.

Mineral abbreviations in text, tables, and figures are after Kretz (1983), except for alumino-silicate (Als), amphibole (Amp), and water (W).

2. Geological outline

An exposure of the Archean to early Paleoproterozoic Pre-Sayan basement in the southwestern margin of the Siberian Platform, separated from the late Proterozoic and Paleozoic complexes (East Sayan fold belt) to the southwest by the Main Sayan Fault (Fig. 1a), is composed of granitic rocks including enderbite and charnockite, amphibolite- to HP granulite-facies gneiss, mafic and ultramafic rocks, carbonate rocks, and pelitic-psammitic rocks, and is intruded by post-collisional granitic rocks of the late Paleoproterozoic Sayan complex (e.g., Eskin et al., 1988; Khiltova, 1993). The Pre-Sayan basement is divided into the Sharyzhalgai, Onot, Urik–Iy, and Biryusa complexes from east to west by strike-slip and high-angle normal faults (Fig. 1a): The two eastern complexes contain sparse pelitic-psammitic rocks while granitic rocks and high-grade metamorphic rocks are predominant, compared with the two to the west. These two eastern complexes have attracted a great deal of attention because they contain well preserved Archean protoliths that underwent Paleo-

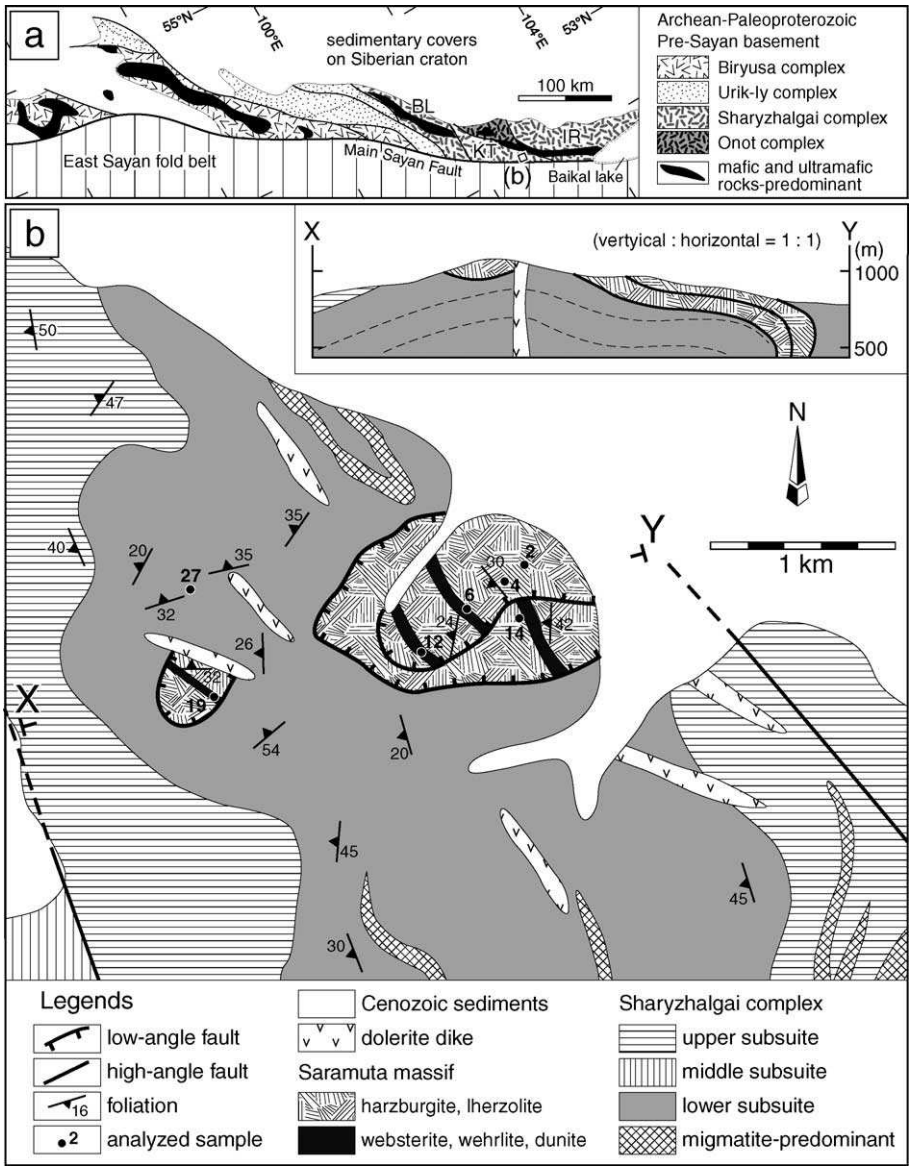

Fig. 1. (a) Sketch map showing the Archean-Paleoproterozoic Pre-Sayan basement in the southwestern margin of the Siberian craton, modified after Khiltova (1993). A small open square indicates a location of (b). BL, Bulun; IR, Irkut; and KT, Kitoy. (b) Geologic map and cross-section around the Saramta massif in the Kitoy block of the Sharyzhalgai complex. Localities of analyzed samples (98O2, 4, 6, 12, 14, 19, and 27) are also shown.

proterozoic HP granulite- or eclogite-facies metamorphism (Aftalion et al., 1991; Khiltova, 1993; Sharkov et al., 1995, 1996; Gornova and Petrova, 1999; Sklyarov et al., 1998, 2001).

The Sharyzhalgai complex is subdivided into fault-bounded blocks of Irkut, Kitoy, and Bulun from east to west (Fig. 1a). These blocks consist mainly of granitic gneiss and migmatite, which enclose amphibolite- to HP granulite-facies mafic and ultramafic rocks, and minor metacarbonate and metapelite; it is from the Kitoy and Bulun blocks that records of eclogite-facies metamorphism have been confirmed

(Khiltova, 1993; Sharkov et al., 1995; Sklyarov et al., 1998; Gornova and Petrova, 1999).

The study area is in the Kitoy block. The gneiss and associated rocks there are divided into three sub-suites; upper, middle, and lower, based on their structural position and mineral parageneses (Fig. 1). The structural upper sub-suite consists of granodioritic gneiss with Bt + Pl + Qtz ± Amp ± Cpx, intercalations of mafic gneiss with Bt + Amp + Cpx + Pl ± Qtz, and rare marble with Di + Dol + Cal ± Pl. The middle sub-suite is characterized by charnokite gneiss with Grt + Opx + Bt + Pl + Qtz ± Crd ± Sil ± Kfs, and mafic granulite with Bt + Cpx + Opx + Pl ± Grt ± Qtz. The lower sub-suite consists of enderbite and charnockite with Cpx + Bt + Pl + Qtz, Grt + Bt + Pl + Qtz ± Opx ± Kfs, or Grt + Mag + Qtz + Pl gneisses, amphibolite, Cpx + Opx + Pl ± Amp ± Bt ± Qtz mafic granulite, and minor quartzite. The ultramafic bodies occur as small lenses or thin slabs within the lower sub-suite, and are separated from the host gneisses by low-angle shear zones. Migmatite veins on various scales occur within all three sub-suites, although only map-scale units of migmatites are illustrated in Fig. 1b.

The gneisses contain close to tight folds and related axial planar structures, with the predominant foliation dipping at gentle to moderate angles toward the southwest; both ultramafic bodies and the host rocks, including migmatitic gneisses, are involved in this regional structure; they are intruded by post-folding dolerite dikes (Fig. 1b).

The Saramta massif is the ultramafic body with the largest aerial extent (up to 1 km in diameter). It is composed of harzburgite with minor lherzolite, and alternating intercalations of dunite and websterite. The ultramafic rocks are generally massive; however, harzburgite often exhibits a banded structure defined by Opx-rich layers 0.5–5 cm (rarely up to 20 cm) in thickness. At some localities, the harzburgites are subjected to ductile deformation resulting in close folds, and rarely in mylonitic textures.

3. Petrography

3.1. Peridotites

The Saramta peridotites include Spl-harzburgite, Spl-lherzolite, and dunite; the first two often preserve protogranular textures composed mainly of Opx, pale-green Cpx, and Ol. These grains surround dark-brown Spl with holly-leaf like or lenticular shapes. The Spl-peridotites are variably sheared and altered, resulting in secondary Srp, Chl, Mag, Ol, and Amp. Most Cpx have tiny laths of Opx exsolutions in their core domains. The matrix Opx often display kink-bands, and contain tiny Spl exsolutions in the cores. Some Spl include Opx and Ol in their rims. Rare mylonitized harzburgites are characterized by coarse-grained porphyroclastic Opx and Cpx set within a matrix composed of fine-grained Ol neoblasts and Spl seams. The porphyroclastic Cpx have dusty cores with abundant Opx or Spl exsolutions.

The dunites, closely associated with Grt-websterites, are composed of Ol and Spl, and secondary Srp and Mag. Anhedral Ol grains are highly serpentinized. Brown Spl show irregular shapes and are scattered throughout the matrix.

3.2. Garnet-websterite

Grt-websterites occur as lenses or layers with thickness less than a few meters that commonly alternate with dunite layers. They are generally massive and

Fig. 2. Back-scattered images of the garnet-websterite (a, b, and c) and photomicrographs of the granitic gneiss (d, e, and f) in the Sharyzhalgai complex. (a) Textures of garnets and orthopyroxenes. A field of (b) is also shown. Orthopyroxenes (gray) occur around garnet grains (light gray), but are often separated from the garnets by kelyphites. Bright rims of the garnet, in contact with the orthopyroxene or the kelyphite, are highly depleted in pyrope content. An orthopyroxene inclusion (dark gray) in the garnet is rich in MgO, compared with that in matrix. (b) Kelyphites of plagioclase, orthopyroxene, and spinel surrounding garnet grain. The garnet rim is decomposed into orthopyroxene and plagioclase, followed by exsolutions of vermicular spinels. A margin of clinopyroxene is replaced by pargasite. (c) Composite inclusions of clinopyroxene and pargasite in garnet. (d) A part of garnet porphyroblast in matrix of quartz, plagioclase, biotite, and orthopyroxene (plane-polarized light). In the garnet porphyroblast, its core with abundant inclusions is surrounded by inclusion-poor or homogeneous mantles. (e) Texture of biotite inclusions in the garnet porphyroblast (crossed-nicol). The biotite inclusions are partly armored by vermicular orthopyroxenes, and further by plagioclases. (f) Texture of garnet and orthopyroxene in migmatized gneiss (plane-polarized light). Garnet porphyroblasts are separated from matrix quartz by walls of plagioclase and orthopyroxene.

composed mainly of pale-green Cpx, pale-brown Opx, and pale-red Grt. Trace amounts of Ol occur as small clusters surrounded by Cpx and Opx, but never coexist with Grt. Occasionally porphyroclastic pyroxenes occur within the matrix of fine-grained pyroxene neoblasts.

The Grt-websterites have been variably retrogressed under hydrous and relatively low-pressure (LP) con-

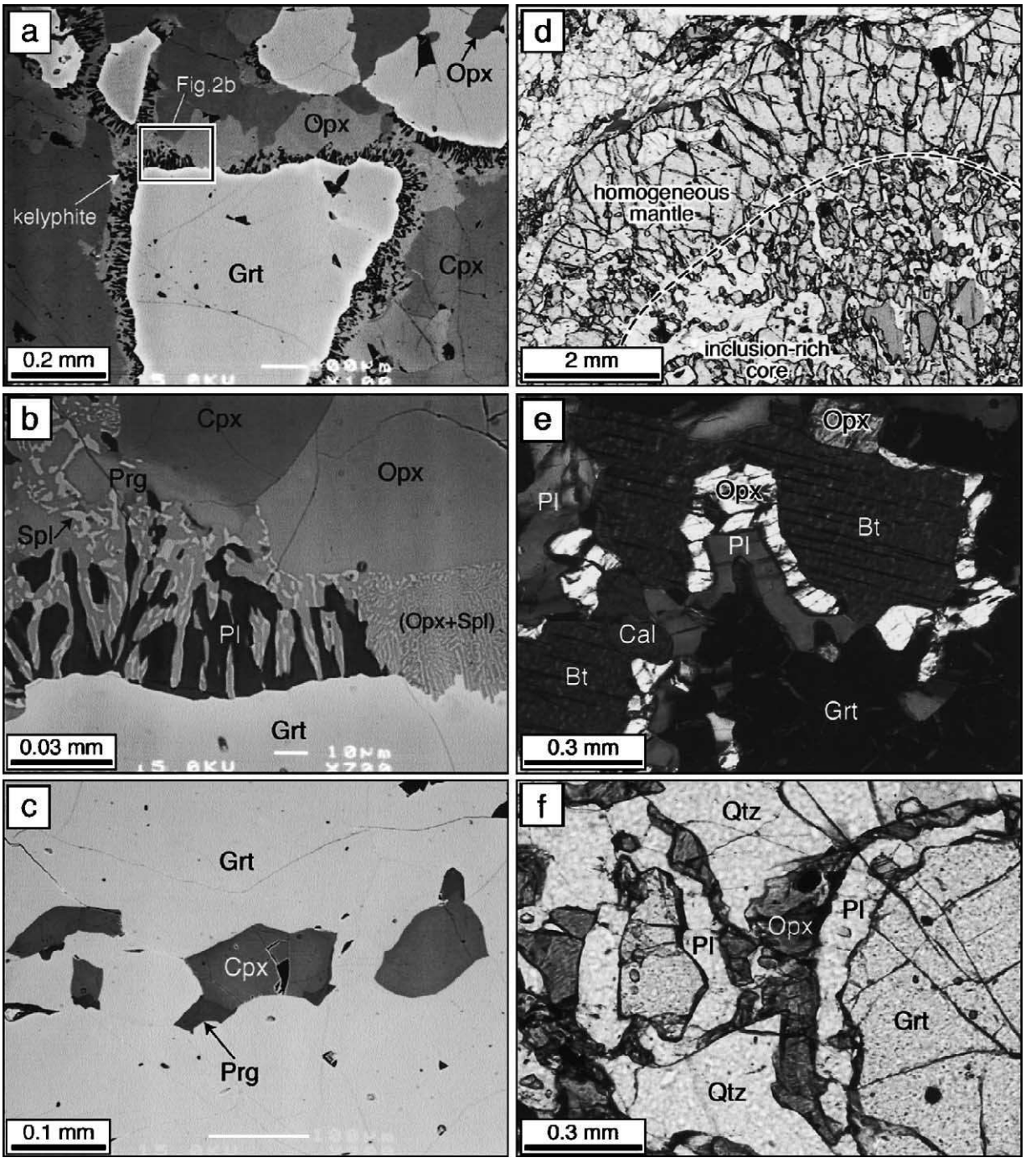

ditions, with minerals such as Amp, Bt, and Chl, and Cal within shear bands or forming veinlets. Less retrogressed Grt-websterites show hypidomorphic granular textures and range in grain size from 0.4 to 1.2 mm. Grt grains are anhedral even in the least altered samples, and are partly rimmed by thin kelyphites with Pl + Opx ± Spl (Fig. 2a and b). Matrix Opx tend to occur near Grt, and are often in direct contact with Grt without kelyphite. Most Cpx occurs in contact with Grt and Opx, and are rarely rimmed by Amp. In places, Opx, Cpx, and Amp inclusions are observed within Grt grains (Figs. 2c and 6); Cpx and Amp often form composite inclusions (Fig. 2c). Moderately retrogressed Grt-websterites tend to be finer grained. Most Grt are completely armored by kelyphites of Pl + Opx + Spl ± Ol, and are observed as fine-grained relics with irregular shapes. The kelyphites are often surrounded by Bt and Amp. In places, Grt are rimmed by Bt. Cpx often have dusty cores with exsolutions of Opx and Spl. Intense retrogression has produced abundant symplectites with Pl + Ol + Opx ± Spl after Grt. Neoblasts of Spl and Ol are often observed in cores of symplectites without the Grt relics. Irregular-shaped and coarse-grained Cpx have abundant exsolutions of Opx and Spl, and are rimmed by Opx neoblasts.

The above-mentioned varieties and changes in modes of occurrence of constituent minerals suggest that the Grt-websterites have experienced, at least, four stages of (re-)crystallization: stage 1 is preserved by inclusions of Cpx+Amp and Opx in Grt, stage 2 by an anhydrous mineral assemblage of Cpx + Opx + Grt within the matrix. In stage 3, firstly, the kelyphite assemblages including Pl without hydrous minerals replace the margins of Grt grains; subsequently they are partly replaced by hydrous minerals including Bt and Amp. Finally, in stage 4, Amp, Chl, and Cal occur within shear planes and veinlets.

3.3. Granitic gneiss and migmatite

Granitic gneisses often show mm- to cm-scale compositional banding, with felsic layers composed of Pl and Qtz with minor Bt, and mafic layers containing Bt, Amp, pyroxene, and Grt; the first three minerals define mineral lineation. The granitic gneisses often enclose amphibolites with Amp ± Cpx ± Pl ± Ep ± Qtz ± Bt and mafic granulites with Cpx + Opx + Pl ± Amp ± Bt ± Qtz ± Grt; they are in sharp contacts with the host gneisses. Leucocratic veins in migmatites occur subparallel or oblique to the foliation of the surrounding gneiss or granulite, and are composed of Pl+Qtz+Bt+Kfs with minor Grt, Ilm, and Ep. Near the contact with the mafic granulites, Bt- and Opx-rich bands are developed in both the leucocratic veins and the granulites.

The granitic gneisses in the upper sub-suite are relatively fine grained, and are characterized by an assemblage of Bt + Pl + Qtz ± Amp ± Cpx ± Kfs with minor Ilm and Ep, while those in the middle sub-suite are coarser grained and have mineral assemblages of Bt + Amp + Cpx + Pl + Qtz ± Grt ± Opx and Bt + Grt + Opx + Pl + Qtz ± Crd ± Sil, with minor Ilm, Kfs, and Zrn.

The lower sub-suite, which contains the ultramafic bodies, is composed of coarse-grained granitic gneisses characterized by assemblages of Bt + Grt + Opx + Pl + Qtz with minor Kfs, Amp, Ilm, Rt, Zrn, and Cal, i.e., charnockite gneisses. Porphyroblastic Grt, ranges from 0.5 mm to 1.2 cm in diameter and has asymmetric tails composed of Opx and Bt. They often show oval outlines, and define their foliation together with Opx and Bt grains. In places, Grt forms lenticular aggregates parallel to the mineral lineation with Bt, Opx, and Pl. Some of the Grt and Bt are replaced by Chl and Ms along their rims. Rarely, coarse Grt porphyroblasts have inclusion-rich cores mantled by homogeneous or inclusion-poor overgrowths (Fig. 2d). The cores contain Bt, Pl, Opx, Kfs, Qtz, and rare Cal inclusions, some of which form composites; although Bt and Kfs are seldom observed within a single composite inclusion. Bt inclusions are often armored by Opx and Pl in the Grt core (Fig. 2e). Composite inclusions bearing Kfs tend to occur in the inclusion-poor mantle of the Grt.

Migmatized gneisses in the lower sub-suite are characteristically high in modal abundance of Grt, and contain Pl, Qtz, Opx, Bt, Kfs, and minor Amp. Among them, Opx and Bt tend to occur in separate domains to each other. In Bt-free domains, Grt porphyroblasts are mantled first by Pl and then by Opx, and are not in direct contact with Qtz (Fig. 2f).

4. Mineral chemistry

Mineral compositions were analyzed using a JEOL JXA8800 electron microprobe at the Department of

Table 1
Representative mineral analyses of the Saramta peridotites in the Sharyzhalgai complex

Sample	98O4				98O14			
Mineral	Ol	Spl	Cpx	Opx	Ol	Spl	Cpx	Opx
SiO_2	41.24	0.02	52.42	56.16	40.88	0.01	53.63	56.50
TiO_2	n.d.	n.d.	0.31	0.08	n.d.	n.d.	n.d.	n.d.
Al_2O_3	n.d.	50.72	5.88	2.83	n.d.	35.28	2.08	2.08
Cr_2O_3	n.d.	18.58	1.13	0.29	0.01	34.52	0.98	0.48
FeO[a]	8.00	12.28	1.87	5.33	6.83	14.88	1.58	4.54
MnO	0.12	0.12	0.05	0.16	0.10	0.23	0.09	0.07
MgO	50.67	18.45	14.44	34.33	51.21	15.26	15.89	34.95
CaO	0.01	n.d.	22.39	0.37	0.04	n.d.	25.44	0.43
Na_2O	0.02	0.04	1.77	n.d.	0.02	0.01	0.58	0.01
K_2O	n.d.	0.02	n.d.	n.d.	n.d.	n.d.	n.d.	n.d.
Total	100.05	100.24	100.26	99.54	99.09	100.18	100.27	99.06
O=	4	4	6	6	4	4	6	6
Si	1.001	0.000	1.889	1.937	0.996	0.000	1.944	1.952
Ti	–	–	0.008	0.002	–	–	–	–
Al	–	1.594	0.250	0.115	–	1.196	0.089	0.085
Cr	–	0.392	0.032	0.008	0.000	0.785	0.028	0.013
Fe^{3+}	0.000	0.016	0.047	0.000	0.008	0.018	0.035	0.000
Fe^{2+}	0.162	0.258	0.009	0.154	0.131	0.340	0.013	0.131
Mn	0.002	0.003	0.002	0.005	0.002	0.005	0.003	0.002
Mg	1.833	0.734	0.776	1.765	1.860	0.654	0.859	1.800
Ca	0.000	–	0.864	0.014	0.001	–	0.988	0.016
Na	0.001	0.002	0.123	–	0.001	0.000	0.041	0.001
K	–	0.001	–	–	–	–	–	–
XMg	0.919	0.728	0.932	0.920	0.930	0.646	0.947	0.932
XCr		0.197	0.114			0.396	0.241	

98O4, spinel-lherzolite; 98O14, spinel-harzburgite; n.d., not detected; XMg, $Mg/(Mg + Fe^*)$; XCr, $Cr/(Cr + Al)$.
[a] Total iron as ferrous.

Earth and Planetary Sciences, Tokyo Institute of Technology. X-ray intensities were reduced using an oxide ZAF correction scheme. Localities of analyzed samples and representative mineral analyses are shown in Fig. 1b, and Tables 1–3 . Ferric iron contents were estimated based on charge balance constraints for Ol and Spl (O=4), pyroxenes (O=6) and Grt (O=12). Those in Amp were calculated on the assumption: $Si + Al + Ti + Fe + Mn + Mg = 13$ for O=23. For Bt and Pl, total iron is assumed ferrous and ferric, respectively.

4.1. Peridotites

Chemical compositions of coexisting Ol and Spl in the Saramta peridotites with protogranular textures are similar to other mantle-derived Spl-peridotites, and plot within or near a narrow band (Fig. 3), the olivine-spinel-mantle-array (OSMA), in terms of XMg ($=Mg/(Mg + Fe_{total})$) in Ol and XCr ($=Cr/(Cr + Al)$) in Spl (Arai, 1987, 1990, 1994). The Ol compositions either represent high-XMg varieties within the OSMA or plot to the higher XMg side off the OSMA. They plot near the fields defined by peridotite xenoliths in African kimberlites (e.g., Boyd and Nixon, 1975) and by xenoliths from oceanic hot-spots (e.g., Sen, 1988; Tracy, 1980), but not within the field defined by ocean-floor peridotites (e.g., Dick and Bullen, 1984; Dick et al., 1984; Michael and Bonatti, 1985).

Cpx in the Saramta peridotites are highly magnesian Cr-diopsides (Table 1 and Fig. 4). The Al_2O_3 contents are 5.1–6.1 wt.% in lherzolite, while 2.1–2.3 wt.% in harzburgite; they tend to decrease from core to rim. Opx are relatively aluminous enstatite (Table 1 and Fig. 4). The Al_2O_3 contents are 2.1–3.4 wt.%, and slightly lower at the rims.

Table 2
Representative mineral analyses of the Saramta garnet-websterites in the Sharyzhalgai complex

Sample	98O12					98O19						
Mineral	Grt c	Grt r	Cpx c	Opx c	Opx r	Grt cia	Grt cib	Grt c	Grt r	Grt rk	Cpx i	Cpx c
SiO_2	39.77	39.48	53.61	54.83	53.47	39.43	39.80	39.53	39.92	39.19	53.02	51.79
TiO_2	0.10	0.01	0.06	0.03	0.01	0.06	0.01	0.03	0.08	n.d.	0.14	0.17
Al_2O_3	22.05	22.33	1.63	0.74	2.99	22.50	22.69	22.31	22.16	22.27	2.17	5.41
Cr_2O_3	0.30	0.30	0.12	0.04	0.07	0.57	0.43	0.42	0.59	0.42	0.19	0.30
FeO[a]	19.59	19.87	6.60	17.19	17.69	18.89	18.75	17.94	19.75	21.23	6.41	6.66
MnO	0.76	0.76	0.09	0.30	0.29	0.73	0.68	0.78	0.68	0.94	0.15	0.17
MgO	11.40	10.68	14.82	26.31	25.03	11.51	11.84	12.21	11.30	10.03	14.75	13.40
CaO	6.04	6.25	22.43	0.77	0.72	6.36	5.95	5.93	6.30	6.14	23.39	21.19
Na_2O	0.03	n.d.	0.75	0.01	0.01	n.d.	0.01	n.d.	0.04	n.d.	0.86	0.89
K_2O	n.d.	0.02	n.d.	n.d.	n.d.	n.d.	n.d.	n.d.	n.d.	n.d.	n.d.	0.03
Total	100.02	99.70	100.11	100.21	100.28	100.06	100.16	99.16	100.81	100.22	101.07	100.01
O=	12	12	6	6	6	12	12	12	12	12	6	6
Si	2.985	2.981	1.970	1.985	1.939	2.952	2.971	2.972	2.976	2.962	1.928	1.906
Ti	0.006	0.000	0.002	0.001	0.000	0.003	0.000	0.002	0.004	–	0.004	0.005
Al	1.950	1.987	0.071	0.032	0.128	1.986	1.996	1.977	1.947	1.983	0.093	0.235
Cr	0.018	0.018	0.003	0.001	0.002	0.034	0.025	0.025	0.035	0.025	0.006	0.009
Fe^{3+}	0.056	0.034	0.036	0.000	0.000	0.069	0.038	0.051	0.063	0.067	0.099	0.000
Fe^{2+}	1.173	1.221	0.167	0.521	0.536	1.114	1.132	1.077	1.169	1.275	0.096	0.205
Mn	0.048	0.048	0.003	0.009	0.009	0.046	0.043	0.050	0.043	0.060	0.005	0.005
Mg	1.275	1.202	0.812	1.420	1.353	1.285	1.317	1.369	1.255	1.130	0.799	0.735
Ca	0.486	0.506	0.883	0.030	0.028	0.511	0.475	0.478	0.503	0.497	0.911	0.835
Na	0.004	–	0.054	0.000	0.001	–	0.001	–	0.005	–	0.060	0.063
K	–	0.002	–	–	–	–	–	–	–	–	–	0.001
XMg	0.509	0.489	0.800	0.732	0.716	0.521	0.530	0.548	0.505	0.457	0.804	0.782

Sample	98O19							98O2[b]			98O6[b]	
Mineral	Opx i	Opx c	Opx r	Opx k	Prg I	Prg k	Pl k	Ol s	Opx s	Cpx	Ol	Spl s
SiO_2	54.48	54.44	52.98	51.85	42.58	41.22	50.98	38.46	54.92	49.69	39.59	0.02
TiO_2	0.03	0.04	n.d.	n.d.	2.22	3.03	0.03	n.d.	0.04	0.28	n.d.	0.03
Al_2O_3	1.57	1.26	3.38	3.92	16.31	15.53	31.26	0.01	1.38	5.23	n.d.	60.91
Cr_2O_3	0.09	0.11	0.13	0.12	0.61	0.35	0.03	0.04	0.04	0.04	n.d.	6.94
FeO[a]	15.65	16.73	16.24	18.62	7.96	10.96	0.84	20.05	12.63	5.26	15.76	15.99
MnO	0.21	0.21	0.27	0.45	0.03	0.12	0.02	0.36	0.44	0.19	0.24	0.14
MgO	27.63	26.45	26.11	23.78	13.76	12.38	0.45	40.29	29.16	14.93	43.97	16.72
CaO	0.67	0.72	0.74	0.58	11.16	12.39	14.43	0.08	0.38	23.03	n.d.	n.d.
Na_2O	0.05	0.07	0.04	n.d.	2.52	2.62	3.80	n.d.	n.d.	0.53	n.d.	0.01
K_2O	n.d.	n.d.	0.02	n.d.	0.95	1.12	0.03	0.02	n.d.	n.d.	0.01	n.d.
Total	100.38	100.03	99.92	99.32	98.08	99.72	101.87	99.30	98.98	99.17	99.57	100.77
O=	6	6	6	6	23	23	8	4	6	6	4	4
Si	1.951	1.970	1.914	1.910	6.073	5.958	2.298	0.997	1.971	1.830	1.002	0.001
Ti	0.001	0.001	–	–	0.238	0.330	0.001	–	0.001	0.008	–	0.001
Al	0.066	0.054	0.144	0.170	2.742	2.646	1.660	0.000	0.058	0.227	–	1.860
Cr	0.003	0.003	0.004	0.004	0.069	0.040	0.001	0.001	0.001	0.001	–	0.142
Fe^{3+}	0.031	0.006	0.027	0.006	0.288	0.000	0.032	0.006	0.000	0.135	0.000	0.000
Fe^{2+}	0.437	0.501	0.463	0.567	0.662	1.325	–	0.429	0.379	0.027	0.333	0.346
Mn	0.006	0.006	0.008	0.014	0.003	0.015	0.001	0.008	0.013	0.006	0.005	0.003
Mg	1.475	1.427	1.407	1.306	2.925	2.667	0.030	1.557	1.560	0.820	1.658	0.646
Ca	0.026	0.028	0.029	0.023	1.706	1.919	0.697	0.002	0.015	0.909	–	–
Na	0.004	0.005	0.003	–	0.696	0.734	0.332	–	–	0.038	–	0.001
K	–	–	0.001	–	0.172	0.206	0.002	0.000	–	–	0.000	–

Table 2 (*Continued*)

Sample	98O12					98O19						
Mineral	Grt c	Grt r	Cpx c	Opx c	Opx r	Grt cia	Grt cib	Grt c	Grt r	Grt rk	Cpx i	Cpx c
XMg	0.759	0.738	0.741	0.695	0.755	0.668		0.782	0.805	0.835	0.833	0.651
XAn							0.676					

c, core; cia, core contact with inclusions of clinopyroxene and pargasite; cib, core contact with inclusion of orthopyroxene; r, rim; rk, rim contact with kelyphite; i, inclusion in garnet; k, in kelyphite; s, in symplectite; XAn, Ca/(Ca + Na + K). Other abbreviations are same as those in Table 1.

[a] Total iron as ferrous.

[b] Highly retrogressed and garnet-free samples.

4.2. Garnet-websterite

Cpx in the Grt-websterites are Al-diopside (Al_2O_3 = 1.58–6.17 wt.%; XMg = 0.78–0.83). Those from the coarse-grained Grt-websterites are higher in CaO, and those from the intensely retrogressed websterites are distinctively high in XMg (0.84–0.91), and are enriched in CaO (Fig. 4). Cpx inclusions in Grt are generally low in Al_2O_3 and slightly high in XMg (Table 2). Irrespective of the mode of occurrence, the Al content increases towards the rims, with mostly constant XMg, and this tendency is especially noticeable for the Cpx grains neighboring Grt grains (Fig. 6).

Table 3
Representative mineral analyses of the Saramta granitic gneiss in the Sharyzhalgai complex

Mineral	Grt ci	Grt c	Grt r	Opx i	Opx c	Opx r	Bt i	Bt c	Bt r	Pl I	Pl c	Pl r
SiO_2	38.53	39.45	39.08	49.85	49.61	49.14	37.93	37.99	38.74	55.75	61.54	61.58
TiO_2	0.02	n.d.	0.03	0.12	0.12	0.15	5.57	3.74	4.67	n.d.	n.d.	0.01
Al_2O_3	22.38	22.95	22.71	6.43	7.09	6.20	16.59	17.02	16.39	27.57	23.12	23.24
Cr_2O_3	n.d.	0.03	0.01	0.04	0.02	0.06	n.m.	n.m.	n.m.	n.d.	n.d.	n.d.
FeO[a]	26.25	24.45	26.68	22.20	21.29	22.34	12.78	10.72	11.90	0.30	0.11	0.12
MnO	0.91	0.82	0.96	0.24	0.28	0.27	n.d.	n.d.	0.03	n.d.	n.d.	0.02
MgO	9.23	11.81	10.47	20.74	20.40	19.90	14.35	15.64	15.35	n.d.	n.d.	n.d.
CaO	2.02	0.90	0.56	0.07	0.02	0.03	n.d.	0.02	0.04	10.57	4.78	5.00
Na_2O	0.02	0.01	0.02	0.03	n.d.	0.02	0.04	0.03	0.07	6.34	8.96	8.57
K_2O	n.d.	0.01	n.d.	n.d.	n.d.	n.d.	9.41	10.90	10.06	0.10	0.51	0.61
Total	99.35	100.42	100.50	99.71	98.83	98.11	96.66	96.05	97.24	100.62	99.01	99.14
O=	12	12	12	6	6	6	11	11	11	8	8	8
Si	2.975	2.970	2.971	1.857	1.855	1.864	2.751	2.768	2.787	2.507	2.763	2.762
Ti	0.001	–	0.002	0.003	0.003	0.004	0.304	0.205	0.253	–	–	0.000
Al	2.037	2.036	2.034	0.282	0.313	0.277	1.418	1.461	1.390	1.461	1.223	1.228
Cr	–	0.002	0.001	0.001	0.000	0.002	–	–	–	–	–	–
Fe^{3+}	0.013	0.024	0.022	0.000	0.000	0.000	–	–	–	0.010	0.004	0.005
Fe^{2+}	1.683	1.516	1.674	0.691	0.666	0.709	0.775	0.653	0.716	–	–	–
Mn	0.059	0.052	0.062	0.008	0.009	0.009	–	–	0.002	–	–	0.001
Mg	1.063	1.325	1.187	1.152	1.138	1.125	1.551	1.699	1.646	–	–	–
Ca	0.167	0.072	0.046	0.003	0.001	0.001	–	0.001	0.003	0.509	0.230	0.240
Na	0.002	0.001	0.002	0.002	–	0.001	0.005	0.004	0.010	0.553	0.779	0.745
K	–	0.001	–	–	–	–	0.870	1.014	0.924	0.005	0.029	0.035
XMg	0.387	0.466	0.415	0.625	0.631	0.614	0.667	0.722	0.697			
XAn										0.477	0.221	0.236

ci, core with inclusions; n.m., not measured. Other abbreviations are same as those in Tables 1 and 2.

[a] Total iron as ferrous.

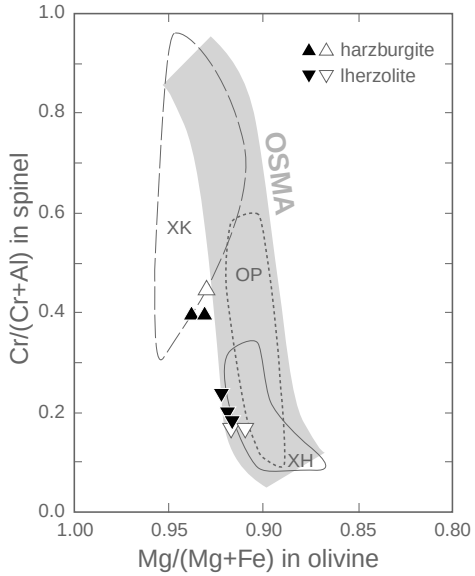

Fig. 3. Compositional variations of spinel and olivine in the Saramta peridotites, with the olivine-spinel-mantle-array (OSMA: Arai, 1987, 1990), shown as a gray thick line. Compositional fields of ocean-floor peridotites (OP: dotted line), kimberlite xenoliths (XK: dashed line), and xenoliths in hotspot basalts (XH: solid line), compiled by Arai (1990), are also shown. Solid and open symbols show data in this study and those from Gornova and Petrova (1999), respectively.

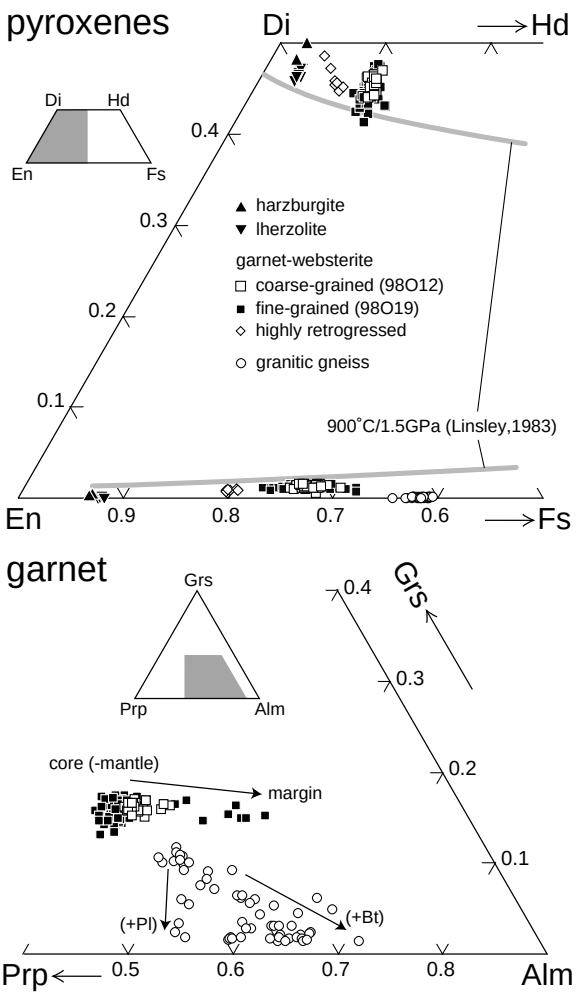

Fig. 4. Compositional variations of pyroxenes (above) and garnet (below) from the Saramta ultramafic rocks and adjacent granitic gneiss in the Sharyzhalgai complex.

Opx are Al-rich enstatites with 0.33–0.84 wt.% CaO. Opx inclusions within Grt are relatively high in XMg (0.74–0.76). Opx from the intensely retrogressed Grt-websterites, including the neoblastic and symplectitic varieties, are distinctively enriched in XMg (0.79–0.81), while the kelyphitic Opx tend to be low in XMg (0.68–0.70) and high in Al_2O_3 (Figs. 4 and 5). For matrix Opx, Al_2O_3 contents (0.74–4.51 wt.%) increase and XMg (0.68–0.75) decrease toward the rims (Figs. 5 and 6). Based on detailed line profiles (Fig. 6), such chemical zoning occurs irrespective of the mode of occurrence, and is most noticeable in Opx in contact with Grt grains and kelyphites.

Grt are pyrope-almandine series; XPrp ($Mg/(Ca + Mg + Fe^{2+} + Mn)$) and XGrs ($Ca/(Ca + Mg + Fe^{2+} + Mn)$) are 0.29–0.46 and 0.13–0.18, respectively. Grt are generally homogeneous in composition, but XPrp is low at the margins and XGrs decreases toward the rims (Figs. 4 and 6; Table 2). Such compositional heterogeneities are common for Grt in contact with kelyphites and for those from the fine-grained Grt-websterite. In a rare case, core compositions of Grt with Cpx and Amp inclusions are slightly low in XPrp and high in XGrs, compared with those of homogeneous Grt grains (Table 2).

Amp in the Grt-websterites are pargasitic, based on Leake et al. (1997), and the inclusions in Grt are high in XMg, compared with those within kelyphites, symplectites and replacing Cpx margins (Table 2). Pl compositions vary from labradorite (XAn = Ca/(Ca + Na + K) = 0.65–0.72) in kelyphites to anorthite (XAn = 0.89–0.94) in sym-

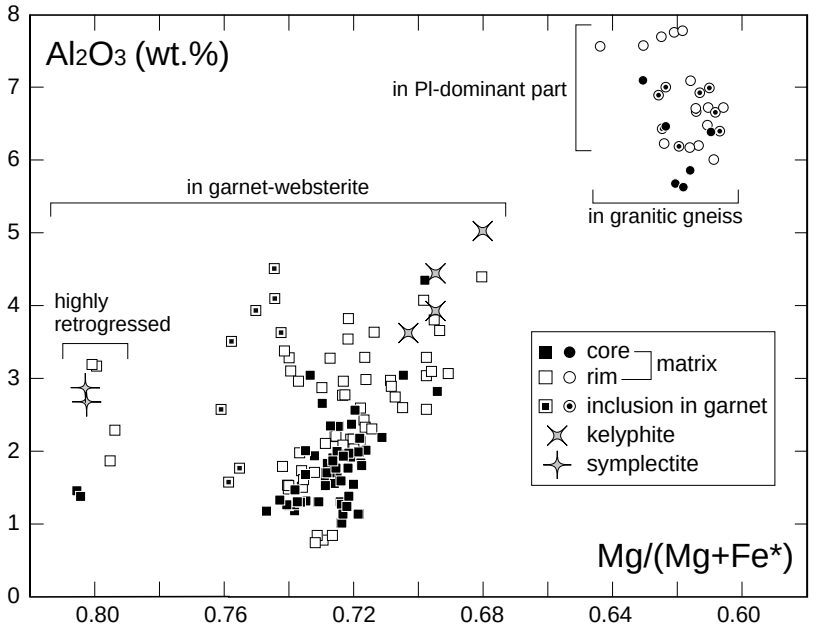

Fig. 5. Compositional variations of orthopyroxenes with different modes of occurrence, from the Saramta garnet-websterites and adjacent granitic gneiss in the Sharyzhalgai complex. Fe* means total iron as ferrous.

plectites (Table 2). Rare matrix Ol exhibit XMg of 0.83–0.84, and symplectite Ol of 0.77–0.79.

4.3. Granitic gneiss

Opx in the granitic gneisses contains Al_2O_3 of 5.6–7.8 wt.%; XMg concentrate in a relatively narrow range (Figs. 4 and 5). Within the matrix, Opx in Pl-dominant parts are slightly elevated in XMg, with Al_2O_3 enrichment in their rims. Opx inclusions within Grt contain Al_2O_3 of 6.1–7.0 wt.%, with XMg similar to those of matrix Opx. Grt are heterogeneous with XGrs (0.01–0.12) and XPrp (0.27–0.45). In general, they show reverse zoning; XGrs and XPrp being higher in their cores. This zonation is especially noticeable at contacts with Bt (Fig. 4). Grt porphyroblasts with abundant inclusions preserve relatively low XPrp compositions within the core (Table 3).

Compositions of Bt and Pl vary by their modes of occurrence. Matrix Bt has a high XMg, while those included within Grt porphyroblasts are low in XMg (Table 3). Rimward decrease of XMg is noted. Matrix Pl are oligoclase (XAn = 0.18–0.24), and the rim compositions are often slightly enriched in XAn (Table 3). In the core of Grt porphyroblast (Fig. 2d and e), Pl between the Grt and Opx inclusions are distinctively high XAn (0.48–0.50; andesine; Table 3).

5. Discussion

5.1. P–T conditions and histories

5.1.1. Peridotites

Primary *P–T* conditions of peridotites are generally poorly constrained since there are few established geothermobarometers for Grt-free peridotites. Additionally, Fe-Mg partitioning between Ol and Spl is easily re-equilibrated upon cooling. Application of the graphical two-pyroxene thermometer (Linsley, 1983) for the Saramta lherzolite yielded temperature conditions of c. 900 °C at 1.5 GPa (Fig. 4). However, assuming that all tetrahedral Al occurs as Ca-tschermak, Cpx within the Saramta peridotites contains Ca-tschermak components of 11.1–13.5 mol% in the lherzolite and 5.6–8.0 mol% in the harzburgite. Based on the petrogenetic grid in the $CaO–MgO–Al_2O_3–SiO_2$ (CMAS) system (Herzberg, 1978), these values for Cpx co-

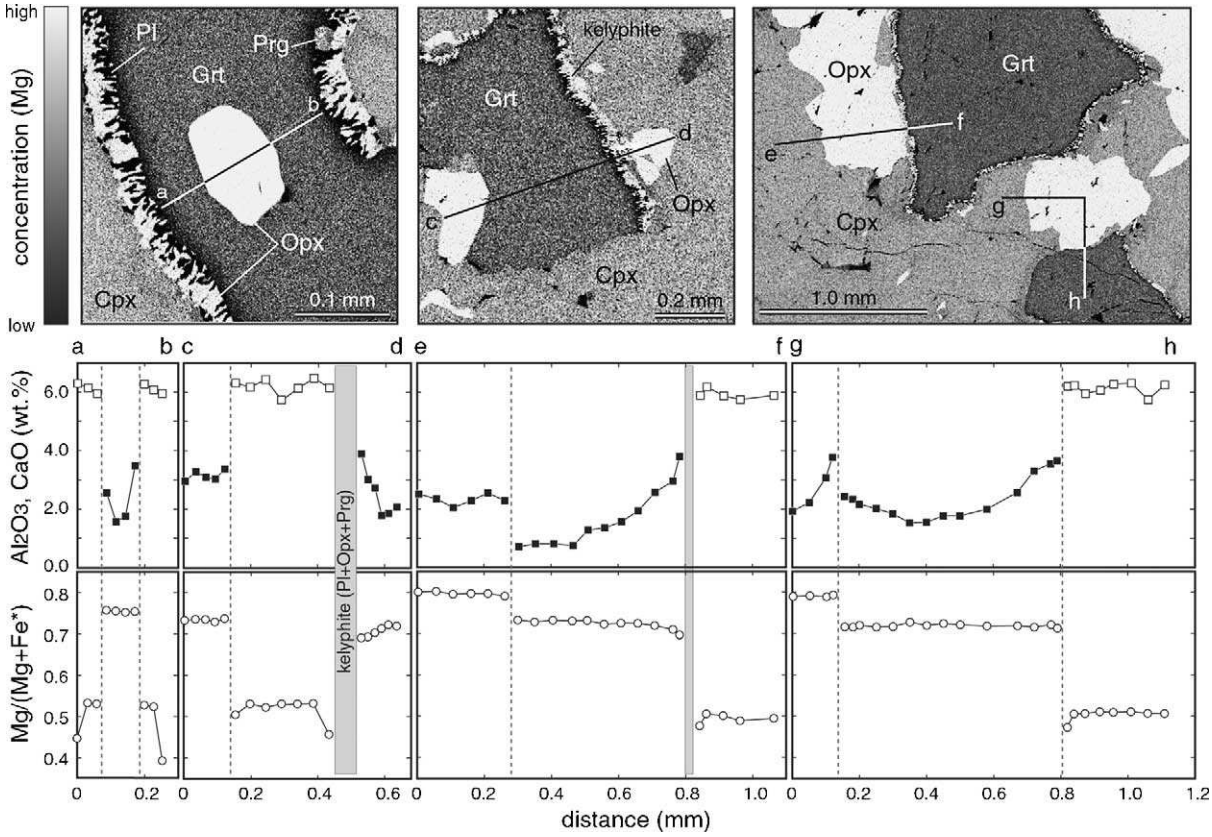

Fig. 6. X-ray composition maps in Mg (top), and line profiles of Al_2O_3 in pyroxenes (solid square) and CaO in garnet (open square; middle), and those of Mg/(Mg + Fe*) (bottom) in pyroxenes and garnet from the Saramta garnet-websterites. Locations of profiles a–b and c–d (98O19), and e–f and g–h (98O12) are shown in the X-ray maps. Fe* means total iron as ferrous.

existing with Opx, Ol, and Spl, yield 1090–1160 °C at 0.8–1.8 GPa for the lherzolite, and 920–1010 °C at 0.7–1.7 GPa for the harzburgite. These temperatures are significantly lower than those previously calculated using re-integrated bulk-mineral compositions (about 1400 °C for Spl-harzburgite: Gornova and Petrova, 1999). Indeed, pyroxenes in the Saramta Spl-peridotites exsolved laths of Opx or Spl during cooling, thus losing their primary magmatic compositions.

Pressure conditions can be inferred assuming that the chemical compositions of Saramta Ol and Spl reflect the igneous petrological characteristics of other mantle-derived Spl-peridotites. Anhydrous melting of mantle peridotites at higher-pressure or higher temperature conditions tends to produce a residual trend with higher XMg in Ol and lower XCr in Spl (Arai, 1994). These relationships suggest that the Saramta peridotites, especially the harzburgites, may have experienced partial melting at HP conditions, corresponding either to near the Grt–Spl transition or to within the Grt stability for the peridotite system.

5.1.2. Garnet-websterite

Several geothermometers, Grt–Opx (Harley, 1984a), Grt–Cpx (Ellis and Green, 1979), Cpx–Opx (Wood and Banno, 1973), Grt–Hbl (Graham and Powell, 1984), Hbl–Pl (Holland and Blundy, 1994), and one geobarometer, Grt–Opx (Harley, 1984b), were applied to the least retrogressed Grt-websterites. Mineral compositions, taken for calculations, are listed in Table 2 and results are summarized in Table 4 and Fig. 7a.

Grt–Opx geobarometers are based on equilibrium reaction (1):

$$Mg_3Al_2Si_3O_{12} = Mg_2Si_2O_6 + MgAl_2SiO_6 \quad (1)$$

pyrope = enstatite + Mg-Tschermak pyroxene

Using THERMOCALC (version 2.7) with an updated version of the internally consistent thermodynamic dataset (Powell and Holland, 1994; Holland and Powell, 1998) and calculated end-member activities of Grt and Opx following Holland and Powell (1998), this equilibrium lay within *P–T* ranges in good agreement with those obtained by Harley (1984b); differences of pressure estimates between the THERMOCALC program and by the calibration of Harley (1984b) were less than 0.2 GPa at 1000 °C.

Textural relationships between Grt and Opx (Figs. 2a and 6) indicate that Al-zoning in Opx formed according to reaction (1). The rimward Al-enrichment is observed not only within matrix Opx but also in Opx inclusions within Grt (Fig. 6). This relationship suggests that Opx compositions with the lowest of Al_2O_3 concentrations (i.e., those within the core of individual grains) should be used in order to obtain pressure conditions as close to the maximum as possible. Even those values should be regarded as minimum estimates.

As noted earlier, stage 1 of the *P–T* history of the Grt-websterites is characterized by inclusions of Cpx+Amp and Opx in Grt, and corresponds to the pre-peak stage. *P–T* calculations using the inclusions Cpx and Prg with higher XMg and lower Al contents, and the Grt core with slightly lower XMg yielded 640–650 °C at a fixed pressure of 1.0 GPa (stage 1a: Fig. 7a). This inclusion assemblage poorly defines pressure conditions, but the Grt stability in the pyroxenite CMAS system (Herzberg, 1978) suggests a minimum pressure estimate of about 0.9 GPa. However, calculations using the core inclusions, Opx with higher XMg and Al contents, and Grt core, gave higher temperatures of about 780 °C at 1.5 GPa (stage 1b: Fig. 7a), suggesting that these mineral inclusions would have retained their assemblages and compositions at different sub-stages during progressive *P–T* increases.

Stage 2 can be regarded as the peak *P–T* stage, as it is characterized by an anhydrous assemblage of Cpx with lower XMg, Opx with lower XMg and Al contents, and Grt with higher XMg. These mineral compositions yielded the highest *P–T* conditions of 1.9–3.0 GPa at 800–1030 °C, with the finer-grained sample (98O19) giving slightly lower pressure and higher temperature estimates than the coarse-grained sample (98O12). In addition, geothermometry using these Cpx compositions give lower temperature estimates for both samples (Fig. 7a). Although the partially retrogressed samples tend to be finer grained, Cpx grains were homogeneous under the microscope and contained no exsolutions detectable through X-ray mapping. However, probe data show that Cpx was clearly zoned with respect to Al (Figs. 5 and 6), and it is probable that core compositions have also been modified during late stage retrogression. Therefore, the conditions calculated at the peak stage of 3.0 GPa at 1030 °C should be regarded as a minimum estimate, and are not inconsistent with previous *P–T* estimates for the Saramta Grt-websterites (2.2–3.8 GPa at c. 1000 °C; Sharkov et al., 1995; Gornova and Petrova, 1999).

During post-peak stage 3, kelyphites with no hydrous mineral replace the margins of Grt grains and are subsequently partly replaced by kelyphites with hydrous minerals such as Bt and Prg. During stages 2 and 3, the composition of matrix Opx was modified to higher Al content and lower in XMg, while Grt was also modified to lower XMg, even for grains without kelyphite rims (Fig. 6). As mentioned before, degrees of compositional modification, especially for Al contents in Opx, are different from each grain, even within one sample. Thus, Opx compositions with the highest of Al_2O_3 concentrations among those from the rims of individual grains in matrix or kelyphite were used to obtain pressure conditions as close to the minimum as possible, although there might be Opx compositions that have truly retained conditions between stages 2 and 3. Geothermobarometry with rim compositions of matrix Grt and Opx resulted in *P–T* estimates of 0.6–0.9 GPa at 750–820 °C, and that with kelyphitic Grt + Opx + Prg + Pl yielded slightly lower pressure conditions around 0.5 GPa at 780–830 °C (stage 3 in Fig. 7a and Table 4). Finally, in stage 4, shear planes and veinlets are characterized by Prg, Chl, and Cal. Additionally, the kelyphites were replaced by Bt. *P–T* conditions at this stage are not well constrained but most likely correspond to lower amphibolite- to greenschist-facies conditions (Fig. 7a).

Table 4
Summary of *P–T* estimates for the Saramta garnet-websterites and adjacent granitic gneiss in the Sharyzhalgai complex

Assemblage	Grt–Opx		Grt–Opx–Cpx				Grt–Opx–Amp		Grt–Opx–Amp–Pl		Grt–Cpx–Amp		Grt–Opx–Pl		Grt–Bt–Pl	
geothermobarometer	H84a + H84b		EG79 + H84b		WB73 + H84b		GP84 + H84b		HB94 + H84b		EG79 + GP84		H84a + ENK91		FS78B + H90	
	T (°C)	*P* (kb)	*T* (°C)	*P* (kb)	*T* (°C)	*P* (kb)	*T* (°C)	*P* (kb)	*T* (°C)	*P* (kb)	*T* (°C)	*T* (°C)	*T* (°C)	*P* (kb)	*T* (°C)	*P* (kb)
98O12 (garnet-websterite)																
Matrix core	940	27.5	816	23.9	864	25.3										
Matrix rim	819	8.9														
98O19 (garnet-websterite)																
Inclusion a											647[a]	641				
Inclusion b	782	14.5														
Matrix core	1000	25.0	991	24.8	894	22.1										
Matrix rim	748	6.1														
Kelyphite	787	4.9					784	4.9	831	5.4						
98O27 (granitic gneiss)																
Inclusion													747	6.0	842	7.8
Matrix core													940	9.3	846	9.0
Matrix rim													816	5.1	773	4.7

Mineral compositions listed in Tables 2 and 3 were used for the calculations. Geothermometers: H84a, Harley (1984a); EG79, Ellis and Green (1979); WB73, Wood and Banno (1973); GP84, Graham and Powell (1984); HB94, Holland and Blundy (1994); FS78B, Ferry and Spear (1978) with Berman (1990)'s garnet solution model; Geobarometers: H84b, Harley (1984b); ENK91, Eckert et al. (1991); H90, R1 calibration of Hoisch (1990).

[a] Calculated at a given pressure of 1.0 GPa.

Integrating these *P–T* estimates allows us to depict a clockwise *P–T* path for the Saramta Grt-websterite, showing a significant *P–T* increase up to the eclogite-facies grade followed by decompression along a steep d*P*/d*T* path; the decompression might be nearly isothermal because of the minimum *P–T* estimates for the stage 3 (a dotted path in Fig. 7a). Finally, the Grt-websterite would experience a nearly isobaric

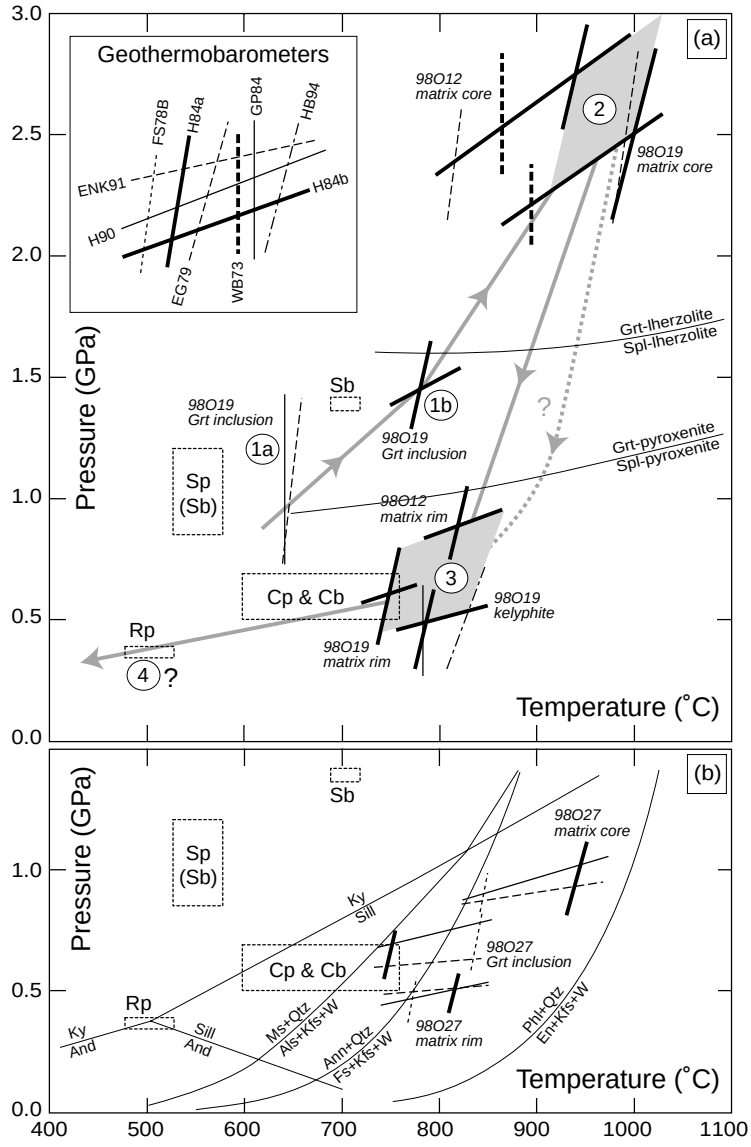

Fig. 7. *P–T* diagram showing estimated metamorphic conditions of the Saramta garnet-websterites (a) and adjacent granitic gneiss (b) in the Sharyzhalgai complex. Garnet–spinel transition curves for lherzolite and pyroxenite are after Herzberg (1978), and the other reaction curves were computed by using a program, THERMOCALC (Powell and Holland, 1994; Holland and Powell, 1998). Results of *P–T* calculations for studied samples are shown as assemblages of two to four reaction curves for geothermobarometry (inset), listed in text and Table 4. A shaded line with arrows is a possible *P–T* path, and numbers in circles represent stages in *P–T* history for the garnet-websterite, described in text. Boxes with dotted lines indicate *P–T* conditions estimated for metamorphic rocks in the Bulun block of the Sharyzhalgai complex (Sklyarov et al., 1998); S, subduction (early) stage; C, collision (late) stage; R, retrograde (latest) stage; b, metabasite; p, metapelite. See text for further explanations.

cooling during the latest retrograde stage. Gornova and Petrova (1999) reported melt inclusions within Grt and pyroxene from the Saramta websterites, and indicated that they were derived by melting at temperatures up to 1300 °C. The Grt-websterites examined in this study would have also experienced much higher temperature conditions prior to the prograde stage. According to Brueckner and Medaris (2000), such a *P–T* history is characteristic of alpine-type, prograde subduction-zone mantle peridotites.

5.1.3. Granitic gneiss

P–T conditions for the granitic gneiss were estimated using the Grt–Opx geothermometer (Harley, 1984a), the Grt–Bt geothermometer of Ferry and Spear (1978) with a Grt solid solution model of Berman (1990), and the Grt–Opx–Pl–Qtz (Eckert et al., 1991) and Grt–Bt–Pl–Qtz (R1 calibration: Hoisch, 1990) geobarometers. Mineral compositions, listed in Table 3, were used for calculations, and the results are shown in Table 4 and Fig. 7b.

Varieties in modes of occurrence and chemical compositions of minerals in the granitic gneiss suggest that their recrystallization can be divided into three stages: pre-peak, peak, and post-peak stages. The pre-peak stage is characterized by the inclusion assemblage in the core of the Grt porphyroblast (Fig. 2d and e). Geothermobarometry using these inclusions Opx, Bt, and Pl, and the core of Grt yield 750–840 °C at 0.6–0.8 GPa. The peak stage is recorded by core compositions of matrix minerals Grt, Bt, and Opx with higher XMg, which gave slightly higher *P–T* estimates of 850–940 °C at 0.9–1.0 GPa.

The inclusion assemblage of Kfs + Opx ± Pl ± Qtz without Bt, occurs predominantly in the mantle of Grt porphyroblasts. This suggests that Kfs could have been derived by the decomposition of Bt in the following reaction:

$$\text{biotite} + \text{quartz} = \text{alkali feldspar} + \text{orthopyroxene} + \text{water} \quad (2)$$

Based on the THERMOCALC calculations, this reaction in the KFASH system indicates *P–T* conditions of c. 800 °C at 0.7 GPa. However, with increasing MgO in the system, the stability field of Bt expands towards higher temperature (Fig. 7b), thus a melt would be produced in the KFMASH system. Integration of this reaction and the geothermobarometry for the pre-peak and peak stages suggests that the granitic gneiss reached peak *P–T* conditions through a progressive *P–T* increase, and that Bt-breakdown by reaction (2) was related to partial melting, i.e., migmatization.

Finally, the post-peak stage is characterized by rim compositions of Grt and Bt with lower XMg, and matrix Opx with lower Al_2O_3. These compositions yielded lower *P–T* estimates of 770–820 °C at c. 0.5 GPa. Within the migmatitic gneiss, Grt porphyroblasts within Bt-absent domains are armored by Pl and Opx, but are not in direct contact with Qtz (Fig. 2f). This texture suggests reaction:

$$\text{grossular} + \text{pyrope} + \text{quartz} = \text{anorthite} + \text{enstatite} \quad (3)$$

In the CMAS system, this reaction has a very gentle positive slope in *P–T* space, and indicates that the migmatitic gneiss also experienced significant decompression after the peak *P–T* conditions.

As a result, the textural and compositional changes of minerals allow us to delineate a *P–T* path for the granitic gneiss, in which the temperature progressively increased up to metamorphic peak conditions, subsequently followed by both pressure and temperature decrease. The replacement of Grt and Bt by Chl and Ms suggests that the gneiss has undergone low-grade metamorphism, most likely in the greenschist-facies.

5.2. P–T evolution of the Sharyzhalgai complex

The *P–T* history of the Saramta Grt-websterites indicates that they were subducted to depths of c. 100 km and subsequently exhumed to mid-crustal depths, followed by rapid cooling. The host gneisses have undergone prograde metamorphism accompanied with migmatization at mid- to lower-crustal levels prior to uplift and cooling at mid-crustal levels. Both lithologies share similar geological histories beginning with the granulite-facies metamorphism at the mid-crust. On the other hand, even though peak *P–T* conditions for Grt-websterites correspond to the Grt stability field in the peridotite system, no HP relic, under subsolidus conditions, has been found within the Spl-peridotites that enclose the Grt-websterites. During granulite-facies migmatization, mineralogical features of both the Spl-peridotites and Grt-websterites

were notably modified. The highly retrogressed Grt-websterites were completely recrystallized in the Spl stability field with the production of Pl + Ol + Opx symplectites with a trace amount of Spl. There is no HP relic of the peak stage of metamorphism in those Grt-websterites. It is likely that the surrounding Spl-peridotites also underwent the complete retrogression, which obliterated the earlier HP mineralogy.

A similar relationship can be observed between coesite- and/or microdiamond-bearing ultrahigh-pressure (UHP) eclogites and their enclosing lower *P* metamorphic rocks in Phanerozoic collisional orogens (e.g., Liou et al., 1994). Commonly, the enclosing lower *P* host rocks apparently have no record of UHP conditions. In addition, UHP eclogites are highly retrogressed back to granulite- or amphibolite-facies mineralogy, where lower *P* overprinting is often accompanied by intense deformation and decompression melting. However, recent studies of mineral inclusions within pressure resistant phases such as Grt and Zrn, have revealed the presence of UHP minerals such as coesite, indicating that retrograded eclogites and even the enclosing gneisses had actually experienced UHP conditions (e.g., summary in Liou et al., 1994). The close spatial association of the Saramta Grt-websterites with Spl-peridotites suggests that at least some of the ultramafic bodies, including the Saramta massif, and probably the host gneisses underwent eclogite-facies metamorphism. However, further investigations are required.

The Bulun block in the western part of the Sharyzhalgai complex is also composed of granulite-facies granite-gneiss containing lenses or layers of ultramafic rocks and metabasites with petrochemical features similar to those in the Kitoy block (i.e., MORB affinities: Sklyarov et al., 1998). The metabasites in the Bulun block record early HP and late LP metamorphism, characterized by assemblages of Grt + Hbl + Pl + Qtz ± Cpx ± Ep ± Rt ± Ilm and Grt + Cum + Pl + Qtz ± Hbl ± Ep ± Ilm, respectively (Sklyarov et al., 1998). Occasionally Cpx are omphacitic, and symplectites of Cpx + Pl after Omp have also been noted in some metabasites with Pl-free matrix, suggesting eclogite- or HP amphibolite-facies conditions (c. 540 °C at c. 1.2 GPa) followed by the LP amphibolite-facies overprinting (up to 600 °C at 0.5–0.6 GPa) to form the symplectites (Sklyarov et al., 1998). Due to including retrograde minerals (i.e., Spn mantling Rt) in the *P–T* calculation, the resulting peak *P–T* conditions (Sklyarov et al., 1998) have been under-estimated. Recalculations using Grt, Hbl, and Pl compositions of the metabasite from the literature (sample number 7010b: Sklyarov et al., 1998) yielded higher *P–T* conditions of 690–720 °C at c. 1.4 GPa (Sb in Fig. 7a). Here, the Grt–Hbl (Graham and Powell, 1984) and Hbl–Pl (Holland and Blundy, 1994) geothermometers, combined with the Grt–Hbl–Pl geobarometer (Kohn and Spear, 1990), and the THERMOCALC program (Powell and Holland, 1994; Holland and Powell, 1998) with end-member activity models of Amp, Grt and Pl by Holland and Powell (1998) were applied. The *P–T* estimates of the HP metamorphism for the metabasites in the Bulun block are comparable with those of the pre-peak stage for the Saramta Grt-websterite, though temperatures are slightly low. Based on the presence of omphacitic Cpx and the possibility that eclogitic assemblages without Pl may have been present originally, we suspect that peak *P–T* conditions of the metabasites were likely to have been higher than estimated here.

Metapelites in the Bulun block also record an early HP and late LP metamorphism, characterized by Grt + Bt + Ky + St and Grt + Bt + Crd + Sil paragenes-es, respectively (Sklyarov et al., 1998). They differ from the gneisses in the lower sub-suite of the Kitoy block, which do not preserve evidence for the earlier HP metamorphism since they have been completely recrystallized. The mineral assemblage of the middle sub-suite granitic gneiss is comparable with that of the late LP stage of the Bulun block, indicating *P–T* conditions of 600–760 °C at 0.5–0.7 GPa (Sklyarov et al., 1998). During the latest stage, the gneiss and metapelites from both blocks were subjected to similar lower-grade metamorphism (c. 500 °C at 0.4 GPa: Rp in Fig. 7b). Assuming that the LP metamorphism in these two blocks was synchronous, the rocks in the Bulun and Kitoy blocks could represent the lower- and the higher-grade parts of the late LP metamorphism, respectively.

These relations suggest that the HP metamorphism up to the eclogite-facies, followed by granulite-facies LP metamorphism and extensive migmatization, was a general feature in the entire Sharyzhalgai complex; the ultramafic rocks, including the Saramta Grt-websterite, could represent the highest-grade record of the HP metamorphism. Such a *P–T* evo-

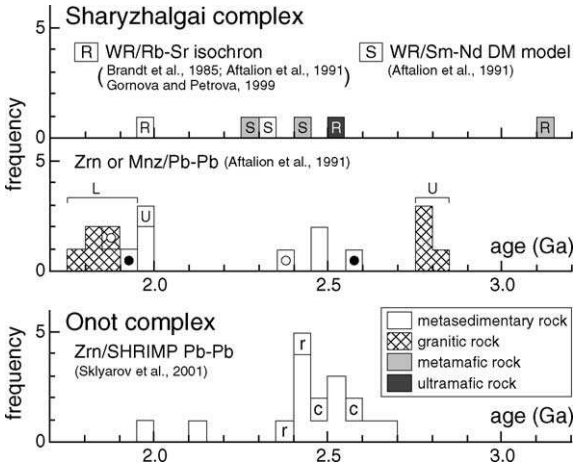

Fig. 8. Frequency distribution diagrams showing isotopic ages of various rock types from the Sharyzhalgai and Onot complexes. Data with small open and solid circles indicate monazite and monazite + zircon ages; the remainders do zircon or whole-rock ages. WR, whole-rock; DM, depleted mantle; L, lower concordia intercept age; U, upper concordia intercept age; c, inherited core with distinct overgrowth; r, overgrowth rim. See also explanations in text.

lution of the Paleoproterozoic Sharyzhalgai complex would be similar to those of Phanerozoic UHP metamorphic collisional orogens.

5.3. Timing of HP metamorphism

A summary of the geochronology of the Sharyzhalgai complex is shown in Fig. 8. Brandt et al. (1985) reported a whole-rock Rb–Sr isochron age (2.51±0.10 Ga with $(^{87}Sr/^{86}Sr)_0$ of 0.7011±0.020) of ultramafic rocks (Ol-pyroxenites) intercalated within gneisses, and suggested that they were mantle-derived materials crystallized at the latest Archean. Aftalion et al. (1991) reported Rb–Sr, Sm–Nd (whole-rock model), and U–Pb (Zrn and Mnz) isotopic ages of gneisses, granulites, and granitic rocks from the Irkut block, and identified the following stages; formation of granitic (c. 2.8 Ga) and mafic (c. 2.4–2.3 Ga) protoliths, early granulite-facies metamorphism (c. 2.5–2.4 Ga), late granulite- to amphibolite-facies metamorphism (c. 2.0 Ga), and finally extensional uplift with intense deformation and formation of granitic rocks (c. 1.9–1.8 Ga), corresponding to granitic intrusions of the Sayan complex (Zrn ^{207}Pb–^{206}Pb ages of 2.00–1.64 Ga: Bryntsev et al., 1985). Aftalion et al. (1991) suggested the presence of earlier metamorphism formed kinzigite (a granulite-facies rock with pelitic composition) (c. 2.5–2.4 Ga). But they also proposed a 2.0-Ga regional granulite-facies metamorphism because the mafic protoliths of granulite-facies rocks give Sm–Nd model ages of 2.4–2.3 Ga. However, Gornova and Petrova (1999) noted that the Sm–Nd model ages might be invalid for estimating protolith ages due to the possibility of an open-system behavior in the Sm–Nd system for Archean rocks affected by much later tectonothermal events including migmatization (e.g., Moorbath et al., 1997). They argued that the mafic protoliths were older, i.e., Middle Archean in age, based on their Rb–Sr whole-rock isochron age of 3.10 ± 0.08 Ga of the granulites. Consequently, there is no need to propose a granulite-facies metamorphism at c. 2.0 Ga. The Middle Archean to the early Paleoproterozoic protoliths of the Sharyzhalgai complex could have been extensively metamorphosed only once under the granulite-facies conditions, recorded in the gneisses and associated rocks, during early Paleoproterozoic times (c. 2.5–2.4 Ga).

On the other hand, the Onot complex, an equivalent to the Sharyzhalgai complex is comprised of granitic rocks including tonalite, migmatitic gneisses, amphibolites, mafic granulites, ultramafic rocks, and minor metacarbonates and metapelites (e.g., Khiltova, 1993). Some of the mafic granulites and ultramafic rocks (Spl-peridotites and Spl- or Grt-websterites), intercalated within the gneisses, record the HP granulite- to eclogite-facies metamorphism with a later lower *P* granulite- to amphibolite-facies overprint (Sharkov et al., 1996; Sklyarov et al., 2001). Sensitive High Resolution Ion MicroProbe (SHRIMP) U–Pb dating of Zrn separated from a Qtz–Grt–Ky metasedimentary rock in the Onot complex provided ^{207}Pb–^{206}Pb ages ranging from 2.67 to 1.99 Ga (17 analyses from 15 grains; Fig. 8). These ages were interpreted as reflecting protolith formation at 2.67–2.52 Ga (seven grains), HP metamorphism at 2.48–2.41 Ga (seven grains), and resetting to the youngest age of 1.99 Ga during late tectonothermal events related to granitic intrusions of the Sayan complex, extensively developed in other complexes of the Pre-Sayan basement (Sklyarov et al., 2001).

Sklyarov et al. (2001) confirmed Ky inclusions in Zrn grains from the Qtz–Grt–Ky metasedimentary

rock, suggesting that at least some of the Zrn grains were of HP metamorphic origin. The early Paleoproterozoic HP metamorphism is still debatable because relationships between distribution of the inclusions and internal textures in actually dated Zrn grains are unclear, although inherited cores (2.6–2.5 Ga) with distinct overgrowths (c. 2.4 Ga) have been confirmed from some of the dated Zrn grains (Fig. 8; M. Fanning, personal communication).

In summary, we suggest that the eclogite-facies metamorphism, recorded in the Pre-Sayan basement, would have occurred at the early Paleoproterozoic times, with regarding the SHRIMP results. However, further examinations should be required.

5.4. Tectonic implications

Gornova and Petrova (1999) suggested that mafic and ultramafic rocks (Saramta Spl-peridotites and Grt-websterites) from the Kitoy block of the Sharyzhalgai complex could represent a fragment of the Archean oceanic crust and underlying upper mantle. However, compositional features of Ol and Spl from the Saramta peridotites, as previously described, and characteristics of major, trace and rare earth elements in the Saramta websterites (Gornova and Petrova, 1999) imply that the Saramta ultramafic protoliths were subjected to partial melting and crystallization at HP conditions up to 2 GPa or more. This evidence for derivation at depths over 60 km appear to contradict an origin by mid-ocean ridge magmatism for the ultramafic protoliths, even considering that pre-1 Ga ophiolites are generally thought to be derived from a 14–21 km thick magmatic crust (Moores, 1986, 1993, 2002).

An alternative hypothesis is that the Saramta ultramafic protoliths derived from sub-arc mantle materials. The enrichment of incompatible trace elements in the Saramta ultramafic rocks, interpreted as metasomatic effects by migmatization of the host gneisses in the mid-crust (Gornova and Petrova, 1999), could also be explained by a fluid-related subduction-zone metasomatism (Brueckner and Medaris, 2000). The presence of hydrous mineral inclusion (i.e., Amp) in Grt of the Saramta Grt-websterite (stage 1a) is consistent with derivation from the sub-arc mantle, hydrated by fluids released by dehydration of the subducting slab.

The question is whether or not subduction could have occurred at the end of the Archean. In general, a hotter mantle in the Archean is thought to have resulted in buoyant oceanic lithospheres with thicker oceanic crust, due to higher production rates of melt at spreading centers and thinner underlying lithospheric mantle, because fast convection of a hotter mantle with lower viscosity would have caused the oceanic lithosphere to have less time to thicken and become gravitationally unstable (Sleep and Windley, 1982; Davies, 1992). For example, recent petrological investigations of Early and Middle Archean MORB suggest oceanic crustal thickness of 15–20 km (Ohta et al., 1996; Komiya, personal communication), and a tentative estimate of a 50 Ma-old Early Archean oceanic lithosphere yielded a thickness of around 40 km (Komiya et al., 1999). However, even 40 km thick oceanic lithospheres could have been subducted beneath more buoyant continental lithosphere or even younger oceanic lithosphere. It has been suggested that Early Archean proto-continental crust, composed of tonalite-trondhjemite-granodiorite (TTG), was produced by partial melting of subducting slabs with a dense eclogitic mineralogy (e.g., Rapp et al., 1991). The high geothermal gradients at the Archean subduction zone would lead to melting of eclogitized basaltic oceanic crust, previously hydrothermally altered at the mid-ocean ridge, to form the TTG suite, when the oceanic lithosphere reached beneath the continental or oceanic lithosphere with thickness over 30 km. This model for Archean subduction is shown in Fig. 9a. In this model, the Archean (proto-)continental crust, composed mainly of the TTG suite, would be too buoyant to subduct into the deep mantle, resulting in a direct continent–continent or continent–island arc collision followed by their amalgamation (Fig. 9a). Therefore, there should not be eclogite-facies metamorphism of continental crust.

On the other hand, continental subduction was more likely in the Proterozoic. A Paleoproterozoic subduction zone with a lower geothermal gradient would have enabled a thicker (older) oceanic lithosphere with a thinner oceanic crust to subduct into deep mantle, without melting the oceanic crust (Fig. 9b). The hanging wall of the mantle wedge would have been metasomatized extensively by dehydration fluids from the subducting oceanic crust, in contrast to a small volume of the Archean mantle wedge metasomatized by fel-

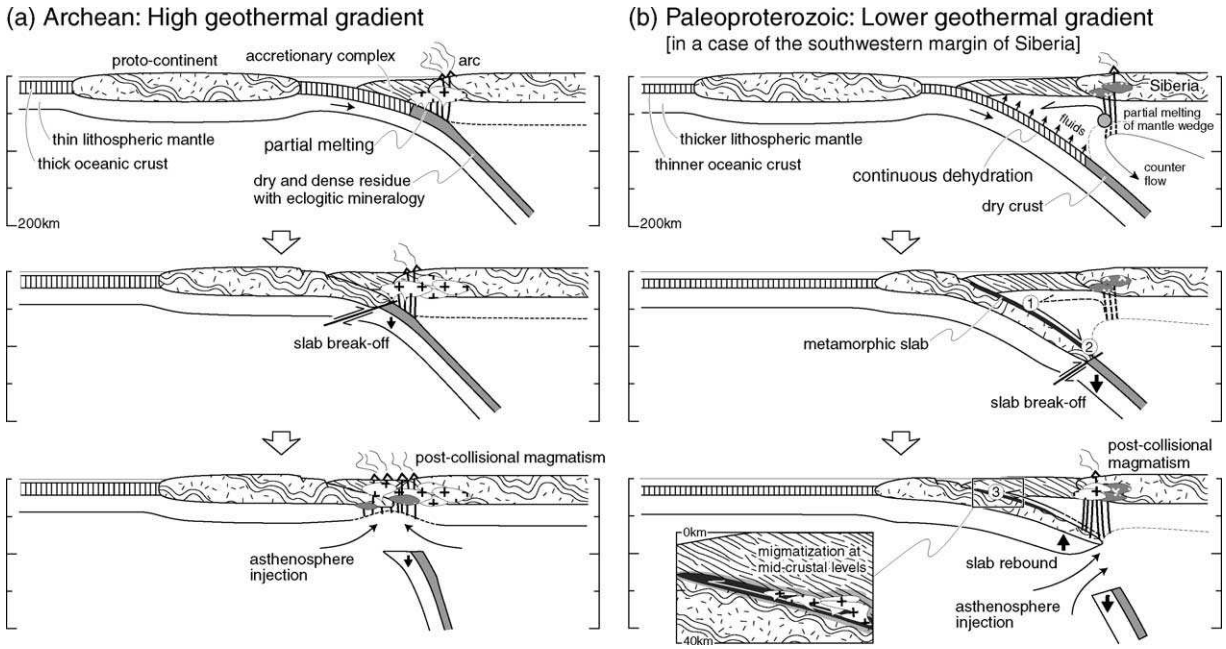

Fig. 9. Schematic cartoons of subduction zones, showing contrasting modes of orogenic processes. (a) Archean. Due to high geothermal gradients, subduction of a thin (young) oceanic lithosphere with a thick oceanic crust results in partial melting of the basaltic oceanic crust to form felsic magma. A highly buoyant continental lithosphere results in breaking-off of the subducting lithosphere at shallow depth, followed by the "head-on" continental collision and related magmatism. There is no subduction of continental crust in this model. (b) Paleoproterozoic (in a case of the southwestern margin of Siberia). Numbers in open circles correspond to metamorphic stages 1, 2, and 3 of the Saramta massif, examined in this study. The Paleoproterozoic subduction zone with lower geothermal gradients enables a thicker (older) oceanic lithosphere with a thinner oceanic crust to subduct into deep mantle. The hanging wall of the mantle wedge is metasomatized by dehydration fluids from the subducting oceanic crust, and a partial melting of the mantle wedge produces mafic island arc magma, where ultramafic protoliths of the Saramta massif (shaded circle) would be generated. With the ingoing subduction of the continental lithosphere, a sub-arc mantle material is trapped into the (proto-)Sharyzhalgai metamorphic slab (stage 1), and subsequently subducts to further depths together with the host supracrustal rocks (stage 2). However, the highly buoyant subduction of the continental lithosphere causes the break-off of the subducting lithosphere at depth; the resultant rebound of the continental lithosphere could help exhumation of the metamorphic slab, and the following asthenosphere injection would trigger a post-collisional magmatism. The exhumed metamorphic slab undergoes tectonothermal overprints with extensive migmatization in mid-crustal levels (stage 3).

sic (TTG) magmas. A partial melting of the hydrated mantle wedge would have produced mafic island arc magma, leaving behind ultramafic protoliths of the type found in the Saramta massif. With the ingoing subduction of the continental lithosphere, this sub-arc mantle material could have been trapped into a metamorphic slab (proto-Sharyzhalgai complex), where it would be refrigerated (stage 1) (Brueckner, 1998), and subsequently subducted to further depths together with the host supracrustal rocks (stage 2) (Brueckner and Medaris, 2000). However, the highly buoyant subduction of the continental lithosphere would have caused the break-off of the subducting lithosphere at depth; the resultant rebound of the continental lithosphere would have caused the exhumation of the metamorphic slab (e.g., Maruyama et al., 1996). The exhumed metamorphic slab would have undergone tectonothermal overprinting with extensive migmatization (decompression melting) at mid-crustal levels (stage 3), and lost much of its original record of deeper-level metamorphism, prior to final exhumation.

It is debatable whether an orogenic process, such as that presented here, could have occurred in Archean or Paleoproterozoic times. But the eclogite-facies metamorphism and *P–T* evolution of the Saramta Grt-websterites and other rocks in the Sharyzhalgai complex suggest that early Paleoproterozoic plate subduction could have transported crustal materials,

rich in H_2O fluids, into great depths (c. 100 km). The Phanerozoic-type plate tectonics, which might have operated in early Paleoproterozoic times, should have caused quite different modes of continental crust formation and mantle metasomatism from those in the Archean times.

6. Conclusions

Integration of petrological and geochronological data from this and other studies for the Sharyzhalgai complex suggests that the Middle Archean to the early Paleoproterozoic protoliths were buried by plate subduction, and were metamorphosed under eclogite-facies conditions. Although the geochronology is ambiguous, we suggest on tectonic grounds that subduction occurred in early Paleoproterozoic times.

The HP assemblages documented in this study suggest that subduction of crustal slabs to depths of c. 100 km occurred in the early Paleoproterozoic, despite the commonly held view that high geothermal gradients in those times would have prevented such a deep subduction. The Sharyzhalgai complex may therefore represent the earliest example of subduction-based tectonics that characterizes the Phanerozoic.

Acknowledgements

We appreciate the careful and constructive reviews by Hannes Brueckner, and an anonymous reviewer, which led to substantial improvement of the manuscript. Mark Fanning provided us useful information for his zircon SHRIMP results from the Onot complex; who is thanked. The first author is grateful to Simon Johnson for improvement of the English and for helpful comments to the early version of manuscript, and to Tsuyoshi Komiya, Akira Ishikawa, Brian Windley, and Shigenori Maruyama for their constructive suggestions and discussion. This study was financially supported in part by a project on Whole Earth Dynamics from the Science and Technology Agency of Japan, by the Russian Foundation for Basic Research (projects 01-05-64000, 00-05-64585, and 00-15-98576), and for support of the Native Science, and by a research fellowship of the Japan Society for the Promotion of Science for Young Scientists to the first author.

References

Arai, S., 1987. An estimation of the least depleted spinel peridotite on the basis of olivine-spinel mantle array. Neues Jahrbuch für Mineralogie, Monatshefte, pp. 347–354.

Arai, S., 1990. What kind of magmas could be equilibrated with ophiolitic peridotites? In: Malpas, J., Moores, E., Panayiotou, A., Xenophontos, C. (Eds.), Ophiolites, Oceanic Crustal Analogues, Proceedings of Symposium “TROODOS 87”, Geol. Surv. Dept. Minist. Agric. Nat. Resour., Nicosia, Cyprus, pp. 557–565.

Arai, S., 1994. Characterization of spinel peridotites by olivine-spinel compositional relationships: review and interpretation. Chem. Geol. 113, 191–204.

Aftalion, M., Bibikova, E.V., Bowes, D.R., Hopgood, A.M., Perchuk, L.L., 1991. Timing of Early Proterozoic collisional and extensional events in the granulite–gneiss–charnockite–granite complex, Lake Baikal, USSR: a U–Pb, Rb–Sr, and Sm–Nd isotopic study. J. Geol. 99, 851–862.

Brandt, S.B., Grudinin, M.I., Lepin, V.S., Men’shagin, Y.V., Kolosnitsyna, T.I., Zarudneva, N.V., 1985. Rubidium-strontium isochron for ultrabasics from the Sharyzhalgai complex (Southwestern Baikal region). Soviet Geol. Geophys. 26, 104–107.

Bryntsev, V.V., Sumin, L.V., Ostapenko, E.I., Pomigalova, N.Y., 1985. Isotopic age of Precambrian granitoids of the northwestern Sayan region. Soviet Geol. Geophys. 26, 46–55.

Berman, R.G., 1990. Mixing properties of Ca–Mg–Fe–Mn garnets. Am. Mineral. 75, 328–344.

Boyd, F.R., Nixon, P.H., 1975. Origins of the ultramafic nodules from some kimberlites of northern Lesotho and the Monastery Mine, South Africa. Phys. Chem. Earth 9, 431–454.

Brueckner, H.K., 1998. Sinking intrusion model for the emplacement of garnet-bearing peridotites into continent collision orogens. Geology 26, 631–634.

Brueckner, H.K., Medaris, L.G., 2000. A general model for the intrusion and evolution of ‘mantle’ garnet peridotites in high-pressure and ultra-high-pressure metamorphic terranes. J. Metamorphic Geol. 18, 123–133.

Davies, G.F., 1992. On the emergence of plate tectonics. Geology 20, 963–966.

Dick, H.J.B., Bullen, T., 1984. Chromian spinel as a petrogenetic indicator in abyssal and alpine-type peridotites and spatially associated lavas. Contrib. Mineral. Petrol. 86, 54–76.

Dick, H.J.B., Fisher, R.L., Bryan, W.B., 1984. Mineralogic variability of the uppermost mantle along mid-oceanic ridge. Earth Planet. Sci. Lett. 69, 88–106.

Eckert, J.O.J., Newton, R.C., Kleppa, O.J., 1991. The ΔH of reaction and recalibration of garnet–pyroxene–plagioclase–quartz geobarometers in the CMAS system by solution calorimetry. Am. Mineral. 76, 148–160.

Ellis, J.D., Green, D.H., 1979. An experimental study of the effect of Ca upon garnet-clinopyroxene Fe–Mg exchange equilibria. Contrib. Mineral. Petrol. 71, 13–22.

Eskin, A. S., Kiselev, A. I., Matison, O. R., 1988. Basite dykes in the Shayzhalgay complex of the Early Precambrian in the Pribaikalye. In: Belichenko, V. G. (Ed.) The Precambrian

Metamorphic Rocks of East Siberia. Nauka, Novosibirsk, pp. 123–128 (in Russian).
Ferry, J.M., Spear, F.S., 1978. Experimental calibration of the partitioning of Fe and Mg between biotite and garnet. Contrib. Mineral. Petrol. 66, 113–117.
Gornova, M.A., Petrova, Z.I., 1999. Mantle peridotites of granulite-gneiss complex as fragments of Archean (?) Ophiolites in the Baikal region (Russia). Ofioliti 24, 223–238.
Graham, C.M., Powell, R., 1984. A garnet-hornmblende geothermometer: calibration, testing and application to the Pelona schist, Southern California. J. Metamorphic Geol. 2, 13–21.
Harley, S.L., 1984a. An experimental study of the partitioning of Fe and Mg between garnet and orthopyroxene. Contrib. Mineral. Petrol. 86, 359–373.
Harley, S.L., 1984b. The solubility of alumina in orthopyroxene coexisting with garnet in $FeO–MgO–Al_2O_3–SiO_2$ and $CaO–FeO–MgO–Al_2O_3–SiO_2$. J. Petrol. 25, 665–696.
Herzberg, C.T., 1978. Pyroxene geothermometers and geobarometer: experimental and thermodynamic evaluation of some subsolidus phase relations involving pyroxenes in the system $CaO–MgO–Al_2O_3–SiO_2$. Geochim. Cosmochim. Acta. 42, 945–957.
Hoisch, T.D., 1990. Empirical calibration of six geobarometers for the mineral assemblage quartz + muscovite + biotite + plagioclase + garnet. Contrib. Mineral. Petrol. 104, 225–234.
Holland, T.J.B., Blundy, J., 1994. Non-ideal interactions in calcic amphiboles and their bearing on amphibole-plagioclase thermometry. Contrib. Mineral. Petrol. 116, 433–447.
Holland, T.J.B., Powell, R., 1998. An internally-consistent thermodynamic dataset for phases of petrological interest. J. Metamorphic Geol. 16, 309–344.
Khiltova, V.Y., 1993. The Kan—Pre-Sayan terrain. In: Rundqvist, D.V., Mitrofanov, F.P. (Eds.), Precambrian Geology of the USSR. Developments in Precambrian Geology, vol. 9. Elsevier, Amsterdam, pp. 365–388.
Kohn, M.J., Spear, F.S., 1990. Two new geobarometers for garnet amphibolites with applications to southeastern Vermont. Am. Mineral. 75, 89–96.
Komiya, T., Maruyama, S., Masuda, T., Nohda, S., Hayashi, M., Okamoto, K., 1999. Plate tectonics at 3.8–3.7 Ga: field evidence from the Isua accretionary complex, Southern West Greenland. J. Geol. 107, 515–554.
Kretz, R., 1983. Symbols for rock-forming minerals. Am. Mineral. 68, 277–279.
Leake, B.E., Woolley, A.R., Arps, C.E.S., Birch, W.D., Gilbert, M.C., Grice, J.D., Hawthorne, F.C., Kato, A., Kisch, H.J., Krivovichev, V.G., Linthout, K., Laird, J., Mandarino, J.A., Maresch, W.V., Nickel, E.H., Rock, N.M.S., Schumacher, J.C., Smith, D.C., Stephenson, N.C.N., Ungaretti, L., Whittaker, E.J.W., Youzhi, G., 1997. Nomenclature of amphiboles: report of the subcommittee on amphiboles of the International Mineralogical Association, commission on new minerals and mineral names. Am. Mineral. 82, 1019–1037.
Linsley, D.H., 1983. Pyroxene thermometer. Am. Mineral. 68, 477–493.
Liou, J.G., Zhang, R., Ernst, W.G., 1994. An introduction to ultrahigh-pressure metamorphism. Island Arc. 3, 1–24.
Maruyama, S., Liou, J.G., Terabayashi, M., 1996. Blueschists and eclogite of the world and their exhumation. Int. Geol. Rev. 38, 485–594.
Michael, P.J., Bonatti, E., 1985. Peridotite composition from the North Atlantic: regional and tectonic variations and implications for partial melting. Earth Planet. Sci. Lett. 73, 91–104.
Moorbath, S., Whitehouse, M.J., Kamber, B.S., 1997. Extreme Nd-isotope heterogeneity in the early Archaean—fact or fiction? Case histories from Northern Canada and West Greenland. Chem. Geol. 135, 213–231.
Moores, E.M., 1986. The Proterozoic ophiolite problem, continental emergence, and the Venus connection. Science 234, 65–68.
Moores, E.M., 1993. Neoproterozoic oceanic crustal thinning, emergence of continents, and origin of the Phanerozoic ecosystem: a model. Geology 21, 5–8.
Moores, E.M., 2002. Pre-1Ga (pre-Rodinian) ophiolites: their tectonic and environmental implications. Geol. Soc. Am. Bull. 114, 80–95.
Ohta, H., Maruyama, S., Takahashi, E., Watanabe, Y., Kato, Y., 1996. Field occurrence, geochemistry and petrogenesis of the Archean mid-oceanic ridge basalts (AMORBs) of the Cleaverville area, Pilbara craton, Western Australia. Lithos 37, 199–221.
Powell, R., Holland, T.J.B., 1994. Optimal geothermometry and geobarometry. Am. Mineral. 79, 120–133.
Rapp, R.P., Watson, E.B., Miller, C.F., 1991. Partial melting of amphibolite/eclogite and the origin of Archean trodjemites and tonalities. Precambrian Res. 51, 1–25.
Sen, G., 1988. Petrogenesis of spinel lherzolite and pyroxenite suite xenoliths from the Koolau shield, Oahu, Hawaii: implications for petrology of the post-eruptive lithosphere beneath Oahu. Contrib. Mineral. Petrol. 100, 61–91.
Sharkov, E.V., Bogina, M.M., Quick, J.E., Mekhonoshin, A.S., 1995. Tectonic blocks of the Precambrian lower crust and upper mantle, Southern Sayan Mountains, East Siberia. Int. Geol. Rev. 37, 81–91.
Sharkov, E.V., Bogatikov, O.A., Kovalenko, V.I., Bogina, M.M., 1996. Early Precambrian lower crustal basic granulites and eclogites from the Kola peninsula and Southern Sayan. Russian Geol. Geophys. 37, 85–102.
Sklyarov, E.V., Gladkochub, D.P., Mazukabzov, A.M., Men'shagin, Yu. V., 1998. Metamorphism of the ancient ophiolites of the Sharyzhalgai nose. Russian Geol. Geophys. 39, 1722–1739.
Sklyarov, E.V., Gladkochub, D.P., Watanabe, T., Fanning, M.K., Mazukabzov, A.M., Men'shagin, Yu. V., Ota, T., 2001. Archean supracrustal rocks of the Sharyzhalgai salient and their tectonic implications. Doklady Earth Sci. 377A, 278–282.
Sleep, N.H., Windley, B.F., 1982. Archean plate tectonics: constraints and influences. J. Geol. 90, 363–379.
Tracy, R.J., 1980. Petrology and genetic significance of an ultramafic xenolith suite from Tahiti. Earth Planet. Sci. Lett. 73, 91–104.
Wood, B.J., Banno, S., 1973. Garnet-orthopyroxene and orthopyroxene-clinopyroxene relationships in simple and complex systems. Contrib. Mineral. Petrol. 42, 109–124.
Zhang, R.Y., Liou, J.G., 1998. Dual origin of garnet peridotites of Dabie-Sulu UHP terrane, eastern-central China. Episodes 21, 229–234.